First Principles Investigation of the Electronic Structure of the Iron Carbide Cation, FeC^+

Demeter Tzeli and Aristides Mavridis*

Laboratory of Physical Chemistry, Department of Chemistry, National and Kapodistrian University of Athens, P.O. Box 64 004, 157 10 Zografou, Athens, Greece

Received: December 20, 2004; In Final Form: June 21, 2005

We have studied 40 states of the diatomic iron carbide cation FeC^+ by multireference methods coupled with relatively large basis sets. For most of the states, we have constructed complete potential energy curves, reporting dissociation energies, usual spectroscopic parameters, and bonding mechanisms for the lowest of the studied states. The ground state is of $^2\Delta$ symmetry, with the first excited state ($a^4\Sigma^-$) lying 18 kcal/mol higher. The $X^2\Delta$ state displays a triple-bond character, with an estimated D_0 value of 104 kcal/mol with respect to the adiabatic products or 87 kcal/mol with respect to the ground-state fragments.

I. Introduction

The present study is a continuation of our work on the electronic structure of the diatomic metal carbides (MC) (neutral or cations),[1] where M is a first row transition metal, and especially of our previous study on FeC.[2,3] In ref 2, we report electronic properties, potential energy curves, and binding characteristics for 41 states of FeC.

Despite the obvious interest in the diatomic metal carbides, which among other things could be considered as conceptual stepping stones for the comprehension of M_nC_m clusters, they have not been studied systematically enough, perhaps because of the increased complexity induced to every molecular system containing first row transition-metal atoms.[1,4]

Concerning the FeC^+ cation, we are aware of three experimental works[5−7] and only one theoretical study based on density functional theory (DFT).[8] In 1986, Hettich and Freiser,[5] using gas-phase photodissociation of $FeCH_2^+$, determined the binding energy of FeC^+ to be 94.5 ± 7 kcal/mol, and more recently, Angeli et al.[6] obtained a value of 84.2 ± 4.1 kcal/mol, employing threshold photoionization of $Fe(CO)_5$. In addition, FeC^+ was observed in the photodissociation and photoionization mass spectrometry of $Fe(CO)_5^{2+}$.[7]

In their very recent theoretical DFT study of Fe_nC, Fe_nC^+, and Fe_nC^- clusters (n = 1−6), Gutsev and Bauschlicher[8] calculated the ground ($X^2\Delta$) and two excited states ($^4\Sigma^-$ and $^6\Pi$) of FeC^+. For the X state, they reported a dissociation energy of 4.86 eV(=112 kcal/mol) and a bond distance (r_e) of 1.53 Å at the DFT(BPW91)/6-311+G* level.

Presently, through high-level multireference variational calculations, we examine a total of 40 states of the FeC^+ cation covering an energy range of about 3.9 eV, correlating adiabatically to $Fe^+[a^6D(3d^64s^1), a^4F(3d^7), a^2G(3d^7)] + C(^3P)$. In particular, from a total of 27 states emerging from the ground-state atoms $Fe^+(^6D) + C(^3P)$, 25 were computed, namely, $^4\Sigma^+[1]$, $^4\Sigma^-[2]$, $^4\Pi[3]$, $^4\Delta[2]$, $^4\Phi[1]$, $^6\Sigma^+[1]$, $^6\Sigma^-[1]$, $^6\Pi[3]$, $^6\Delta[2]$, $^6\Phi[1]$, $^8\Sigma^+[1]$, $^8\Sigma^-[1]$, $^8\Pi[3]$, $^8\Delta[2]$, and $^8\Phi[1]$. A bundle of 14 from a total of 36 states were also examined correlating to $Fe^+(^4F) + C(^3P)$, i.e., $^2\Sigma^+[1]$, $^2\Sigma^-[1]$, $^2\Pi[3]$, $^2\Delta[2]$, $^2\Phi[2]$, $^2\Gamma[1]$, $^4\Gamma[1]$, $^6\Sigma^+[1]$, $^6\Delta[1]$, and $^6\Gamma[1]$. Finally, a single ^2H state is also reported, tracing its lineage to $Fe^+(^2G) + C(^3P)$; the numbers in square brackets indicate the number of states studied in each particular space−spin symmetry. It is interesting to mention, at this point, that the two channels which give rise to the 27 and 36 possible states have an experimental energy separation, $\Delta E[Fe^+(^4F) \leftarrow Fe^+(^6D)]$, of just 0.284 eV (=6.55 kcal/mol).[9]

Following the philosophy of our previous work on FeC[2], we henceforth report potential energy curves (PEC), binding energies, bond distances, electronic separation energies, and common spectroscopic parameters. Some emphasis has been placed on interpreting the bonding process with the help of atomic Mulliken distributions and simple valence-bond-Lewis (vbL) diagrams for the lowest of the states examined, for which we are rather certain of their relative ordering.

In section II, we delineate our computational strategy; in section III, we present relevant atomic numerical results; in section IV, the results of a total of 17 states are discussed in some detail; and in section V, some final conclusions and comments are presented.

II. Computational Strategy

The averaged atomic natural orbital (ANO) basis set of Bauschlicher[10] for Fe, 20s15p10d6f4g, and the quadruple correlation consistent basis set of Dunning,[11] cc-pVQZ = 12s6p3d2f1g, for C were used and were both generally contracted to [7s6p4d3f2g/$_{Fe}$ 5s4p3d2f1g/$_C$] spanning a 139 one-electron Gaussian space.

The inherent multireference character of the FeC^+ states, their diversity of space−spin symmetry, and our desire to construct complete PECs, deemed crucial for a better understanding of bonding, leaves us with only one choice of approach: the complete active space self-consistent field (CASSCF) method coupled with single and double replacement configuration interaction (CASSCF + 1 + 2 = MRCI) to account for additional correlation. The CASSCF wave function is constructed by allotting the 11 "valence" electrons (7 on Fe^+ and 4 on C) to 10 valence orbital functions (4s and 3d on Fe and 2s and 2p on C). The zeroth-order spaces thus created a range from 104 ($^8\Sigma^+$) to 6996 ($^2\Sigma^+$) configuration functions (CF) with corresponding MRCI spaces of about 8×10^6 ($^8\Sigma^-$) to 134×10^6 ($^2\Sigma^+$) CFs. By enforcing the internal contraction technique[12] (icMRCI), the CI spaces are reduced drastically, ranging from 241×10^3 to 2×10^6 CFs, thus making the computations

* Corresponding author. E-mail: mavridis@chem.uoa.gr.

10.1021/jp040765j CCC: $30.25
Published on Web 09/28/2005

TABLE 1: Total Energies (E_h) of $Fe^+(^6D, ^4F)$ and $C(^3P)$, Energy Separation of $^4F \leftarrow {}^6D$ (eV), Ionization Energy (IE, eV) of Fe, and Atomic Spin−Orbit Splittings (SO/J, cm^{-1}) of $Fe^+(^6D, ^4F)$ at Different Levels of Theory

method[a]	$Fe^+(^6D)$	$Fe^+(^4F)$	$^4F \leftarrow {}^6D$	IE	$C(^3P)$
MRCI	−1262.37096	−1262.35721	0.374	7.388	−37.78493
MRCI+Q	−1262.3762	−1262.3660	0.277	7.66	−37.7879
C-MRCI	−1262.71439	−1262.69984	0.396	7.145	
C-MRCI+Q	−1262.7435	−1262.7350	0.231	7.49	
MRCI+DKH	−1271.25637	−1271.23126	0.683	7.482	
MRCI+Q+DKH	−1271.2618	−1271.2403	0.585	7.76	
C-MRCI+DKH	−1271.65075	−1271.62386	0.731	7.218	
C-MRCI+Q+DKH	−1271.6826	−1271.6618	0.565	7.57	
MRCI+CG	−1271.16158	−1271.13483	0.728	7.464	
MRCI+Q+CG	−1271.1668	−1271.1436	0.631	7.74	
C-MRCI+CG	−1271.50379	−1271.4767	0.737	7.225	
C-MRCI+Q+CG	−1271.5329	−1271.5119	0.572	7.57	
exptl[b]			0.248	7.90 ± 0.01	

	$Fe^+(^6D)$			$Fe^+(^4F)$		
SO/J[c]	MRCI	C-MRCI	exptl[b]	MRCI	C-MRCI	exptl[b]
9/2	0.0	0.0		0.0	0.0	
7/2	−385.5	−408.3	−384.77	−567.4	−592.9	−557.48
5/2	−299.8	−317.5	−282.87	−441.4	−461.1	−407.86
3/2	−214.2	−226.8	−194.99	−315.3	−329.5	−279.54
1/2	−128.5	−136.0	−114.40			

[a] +Q, +DKH, and +CG refer to the Davidson correction and scalar relativistic corrections via the Douglas−Kroll−Hess and Cowan−Griffin approaches, respectively. [b] Reference 9. [c] J refers to the spatial + spin angular momentum.

feasible, and with affordable losses in total energies. To estimate core-valence correlation effects, icMRCI calculations were performed including the eight semicore ($3s^23p^6$) electrons of Fe^+ in the CI procedure. These calculations will be referred to as C-MRCI and were done only for the ground state and around the equilibrium geometry. Needless to say, upon inclusion of eight more electrons in the CI, size-nonextensivity errors increase significantly with a synchronous dramatic increase of CFs included in the CI expansion: 1.8×10^9 (uncontracted) to 31.5×10^6 (contracted) CFs for the $X^2\Delta$ state. Moreover, for the ground state only, scalar relativistic corrections using both the Douglas−Kroll−Hess (DKH) one-electron integrals and the perturbative approach using the Cowan−Griffin (CG) operator were obtained, with (C-MRCI+rel) and without (MRCI+rel) the $3s^23p^6$ Fe^+ semicore electrons for the $X^2\Delta$ state. Finally, the spin−orbit splitting for the $X^2\Delta$ state, $\Delta E(X^2\Delta_{5/2} - X^2\Delta_{3/2})$, was calculated via the Breit−Pauli operator.

All calculations were done under C_{2v} symmetry constraints, but all our CASSCF wave functions display correct axial angular momentum symmetry, i.e., $|\Lambda| = 0$ ($\Sigma^{\pm}$), 1 (Π), 2 (Δ), 3 (Φ), 4 (Γ), and 5 (H). This means that Δ and Γ states are linear combinations of A_1 and A_2 symmetries, whereas Π, Φ, and H states are combinations of B_1 and B_2 symmetries; Σ^+ and Σ^- correspond to the A_1 and A_2 symmetry species, respectively. Moreover, the state average approach[13] was applied to those excited states showing interaction with states of the same C_{2v} symmetry nearby. Because of the relatively large number of active electrons, we encountered significant size-nonextensivity problems: 6.5−9 mhartree at the MRCI level, reduced to 1−1.5 mhartree after including the Davidson correction (+Q).[14] The MRCI basis set superposition error (BSSE) was calculated only for the ground $X^2\Delta$ state of FeC^+.

Finally, and only for the ground state, restricted coupled cluster singles and doubles with perturbative connected triples calculations were performed with [C-RCCSD(T)] and without [RCCSD(T)] the Fe^+ semicore $3s^23p^6$ electrons based on CASSCF orbitals.

All calculations were done with the MOLPRO 2000 package.[15]

III. Fe^+ and C Species

The end fragments of the FeC^+ decomposition are clearly Fe^+ and C in all three channels considered here, $Fe^+(a^6D, a^4F, a^2G) + C(^3P)$. Table 1 displays the total energies of $Fe^+(^6D, ^4F)$ and $C(^3P)$, the Fe^+ energy term splitting, $^4F \leftarrow {}^6D$, and the ionization energy (IE) of Fe, [$Fe(^5D) \rightarrow Fe^+(^6D)$], at different levels of theory, along with experimental values.[9] Observe that the theoretical $^4F \leftarrow {}^6D$ energy separation is in good agreement with the experimental one at the MRCI+Q and C-MRCI+Q levels, but the same is not true when scalar relativistic corrections are included in either DKH or CG approximations. Concerning the IE of Fe, the best agreement with experimental values is obtained at the MRCI+Q+DKH level, 7.76 vs 7.90 ± 0.01 eV.

IV. Results and Discussion

Table 2 lists CASSCF, MRCI, and MRCI+Q total energies (E), equilibrium bond distances (r_e), and dissociation energies (D_e) with respect to the adiabatic fragments, total Mulliken charges on Fe^+, harmonic frequencies and anharmonic corrections (ω_e, $\omega_e x_e$), rotational−vibrational couplings (α_e), centrifugal distortions ($\bar{D}_e$), and energy gaps (T_e) of forty states with spatial−spin symmetries $^{2,4,6,8}\Sigma^{\pm}$, $^{2,4,6,8}\Pi$, $^{2,4,6,8}\Delta$, $^{2,4,6,8}\Phi$, $^{2,4,6}\Gamma$, and ^{2}H. Subscripts G and L refer to global and local minima, respectively. Figure 1 contrasts relative energies of all states studied of FeC^2 and FeC^+ covering an energy range of 3.7 and 3.9 eV, respectively, and Figure 2 displays a panorama of all PECs. Each excited state has been labeled with a serial number in front of the symmetry symbol, revealing its absolute energy order with respect to the ground state (X), and a number in parentheses, indicating its absolute order within the same space−spin symmetry manifold. Figures 3−6 show, separately, the PECs according to their spin multiplicity, doublets, quartets, sextets, and octets.

We analyze first the doublets, followed by the quartets, the sextets, and finally, the octets.

A. Doublets. All doublets correlate to the first exited ^4F state of Fe^+, with the exception of the 29^2H state which correlates to $Fe^+(^2G)$, experimentally, 1.993 eV above the ground ^6D term.[9]

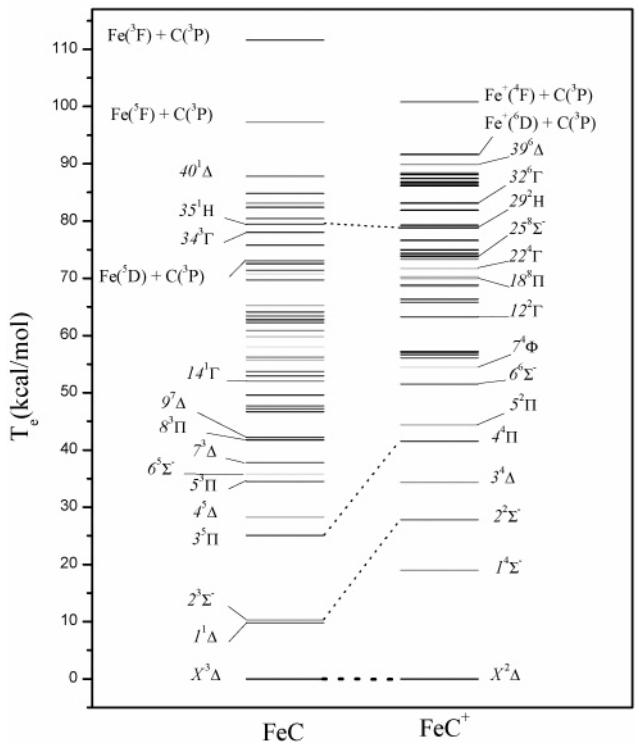

Figure 1. Comparison of the relative energy levels of FeC and FeC^+.

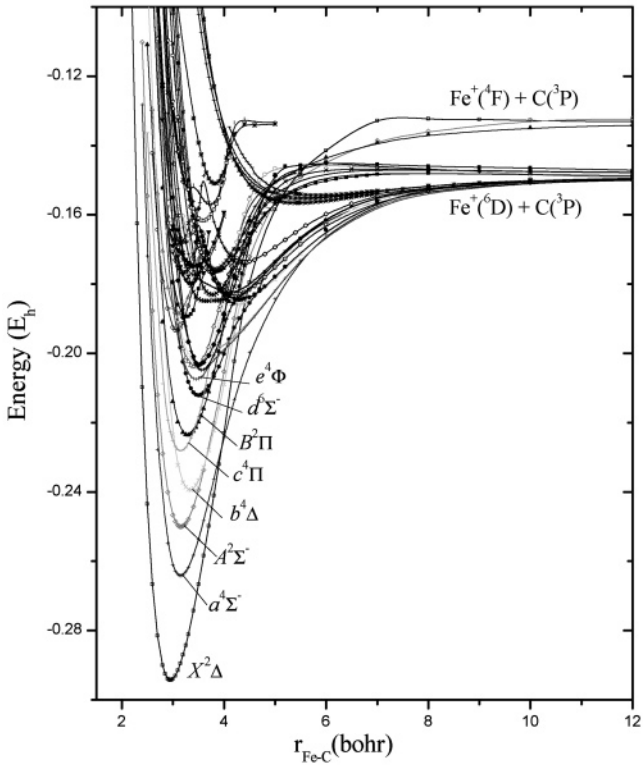

Figure 2. Potential energy curves of 40 states of the FeC^+ cation at the MRCI level of theory. All energies have been shifted by +1300 E_h.

We have obtained results for 11 doublets, 5 of which are discussed in some detail below.

$X^2\Delta$. The ground state of neutral FeC ($X^3\Delta$) is described fairly well by two configurations; see ref 2.

$$|X^3\Delta\rangle_{A_1+A_2} \sim 0.81|1/\sqrt{2}(1\sigma^2 2\sigma^2 3\sigma^1 1\pi_x^2 1\pi_y^2)(1\delta_+^1 1\delta_-^2 + 1\delta_+^2 1\delta_-^1)\rangle = |A_1\rangle + |A_2\rangle$$

(Thenceforth, only valence electrons are counted.)

The $X^3\Delta$ state of FeC correlates to $|^5D;\ M = \pm 2\rangle_{Fe} \times |^3P;\ M = 0\rangle_C$ but, because of an avoided crossing at about 4.5 bohr with the $7^3\Delta(2)$ state, the in situ atoms are Fe($4s^1 3d^7$, ^5F; $M = \pm 2$) + C(^3P; $M = 0$). The two atoms interact attractively through a genuine triple bond of $D_e = 86.7$ kcal/mol and $r_e = 1.581$ Å at the C-MRCI level. *Diabatically*, D_e is 86.7 + $\Delta E(^5F \leftarrow {}^5D)$ = 109.6 kcal/mol or about 107 kcal/mol after BSSE and scalar relativistic corrections.[2] The singly occupied 3σ orbital is practically a 4s atomic function localized on Fe. Removing the $3\sigma(\sim 4s_{Fe})$ e^-, yields the $X^2\Delta$ state of FeC^+, correlating, of course, to $Fe^+(d^7, {}^4F;\ M = \pm 2)$ + C(^3P; $M = 0$) and maintaining this character up to equilibrium. The triple-bonded structure of FeC^+ can be faithfully represented graphically by the following vbL (valence-bond-Lewis) icon in accordance with the leading

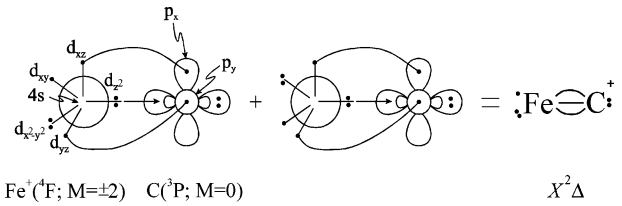

CAS configurations and atomic Mulliken distributions (Fe/C)

$$|X^2\Delta\rangle_{A_1+A_2} \sim 0.85|1/\sqrt{2}(1\sigma^2 2\sigma^2 1\pi_x^2 1\pi_y^2)(1\delta_+^1 1\delta_-^2 + 1\delta_+^2 1\delta_-^1)\rangle$$
$$4s^{0.16}4p_z^{0.11}3d_{z^2}^{1.31}3d_{xz}^{1.23}4p_x^{0.02}3d_{yz}^{1.23}4p_y^{0.02}$$
$$(3d_{x^2-y^2}3d_{xy})^{3.00}/2s^{1.71}2p_z^{0.69}2p_x^{0.73}2p_y^{0.73}$$

The populations above indicate that 0.40 e^- are donated to the empty $2p_\sigma$ carbon orbital, and 0.50 e^- return to the Fe^+ cation through the π route.

At the C-MRCI (C-MRCI+Q) [C-RCCSD(T)] levels, the dissociation energies (D_e) with respect to $Fe^+(^4F)$ + C(^3P) are 101.4 (103) [96.7] kcal/mol at $r_e = 1.553$ (1.557) [1.530] Å. Taking into account scalar relativistic effects via the DKH approximation, we obtain $D_e = 106$ (107) kcal/mol with respect to the $Fe^+(^4F)$ + C(^3P); correcting for ZPE $\equiv \omega_e/2$ (Table 2) and a BSSE of 0.5 kcal/mol, we obtain, finally, $D_0 = 104$ (105) kcal/mol. Practically the same D_e and D_0 values are also obtained via the CG perturbational correction.

With respect to the ground-state fragments, $Fe^+(^6D)$ + C(^3P), the estimated C-MRCI (C-MRCI+Q) [C-RCCSD(T)] D_0 values are reduced by 9 (6) [5] kcal/mol, becoming 89 (94) [88] kcal/mol. These values are in relatively good agreement with the gas-phase experimental result, $D_0 = 94 \pm 7$ kcal/mol, of Hettich and Freise,[5] assuming that they refer to ground-state products. We believe that the $D_0 = 84.2 \pm 4.1$ kcal/mol value of Angeli et al.[6] underestimates the dissociation energy of FeC^+; on the other hand, in the very recent DFT(BPW91)/6-311+G* study by Gutsev and Bauschlicher,[8] the binding energy of the $X^2\Delta$ state of FeC^+ is rather overestimated by about 10 kcal/mol. Finally, the MRCI spin−orbit coupling for the $^2\Delta$ state is $\Delta E(^2\Delta_{3/2} - {}^2\Delta_{5/2}) = A = 729$ cm^{-1}, with $r_e = 1.5690$ and 1.5675 Å for the $^2\Delta_{3/2}$ and $^2\Delta_{5/2}$ components, respectively.

As expected, the binding energies and bond distances between FeC ($X^3\Delta$, diabatic) and FeC^+ ($X^2\Delta$) are similar; indeed, they do not differ by more than 8 kcal/mol and 0.03 Å at the same level of computation.[2]

TABLE 2: Absolute Energies (E_h), Bond Lengths (r_e, Å), and Binding Energies (D_e, kcal/mol) with Respect to Adiabatic Fragments, Harmonic Frequencies (ω_e, cm^{-1}) and Anharmonic Corrections ($\omega_e x_e$, cm^{-1}), Rotational Vibrational Couplings (α_e, cm^{-1}), Centrifugal Distortions ($\bar{D}_e$, cm^{-1}), Mulliken Charges on Fe ($1 - q_{Fe}$), and Energy Separations (T_e, kcal/mol) of FeC^+

state[a]	methods[b,c]	$-E$	r_e	D_e	ω_e	$\omega_e x_e$	α_e (10^{-3})	$\bar{D}_e$ (10^{-6})	q_{Fe}	T_e
$X^2\Delta$	CASSCF	1300.01216	1.576	86.4	860.2	8.41	7.75	1.75	0.07	0.0
	MRCI	1300.29428	1.563	100.8	903.7	5.64	6.43	1.67	0.11	0.0
	MRCI+Q	1300.3136	1.568	101						0.0
	RCCSD(T)	1300.30796	1.542	94.9	970.4					0.0
	MRCI+DKH	1309.19114	1.558	105.7	920.1	5.86	6.40	1.64	0.01	
	MRCI+Q+DKH	1309.2108	1.562	106						
	MRCI+CG	1309.09447	1.561	105.6	910.2	5.75	6.51	1.65	0.11	
	MRCI+Q+CG	1309.1138	1.566	106						
	C-MRCI[d]	1300.63103	1.553	101.4	944.2				0.11	0.0
	C-MRCI+Q[d]	1300.6840	1.557	103.3						0.0
	C-RCCSD(T)[d]	1300.68834	1.530	96.7	1026					0.0
	C-MRCI+DKH[d]	1309.57344	1.551	106.0	928				0.00	
	C-MRCI+Q+DKH[d]	1309.6296	1.555	107						
	C-MRCI+CG[d]	1309.43004	1.552	107.8	932				0.11	
	C-MRCI+Q+CG[d]	1309.4830	1.555	109						
	DFT/BPW91[e]		1.53	112	1027					
	exptl[f]			94 ± 7						
	exptl[g]			84.2 ± 4.1						
$1^4\Sigma^-(1)$	CASSCF	1299.99246	1.675	45.6	740.7	8.06	7.06	1.64	0.08	12.4
	MRCI	1300.26406	1.667	72.2	789.2	5.05	5.43	1.49	0.12	19.0
	MRCI+Q	1300.2842	1.671	76						18
	DFT/BPW91[e]		1.64		831					16.6
$2^2\Sigma^-(1)$	CASSCF	1299.98194	1.695	67.4	759.1	4.14	4.81	1.45	0.07	19.0
	MRCI	1300.25002	1.670	73.1	801.6	4.14	4.92	1.42	0.13	27.8
	MRCI+Q	1300.2694	1.672	73						28
$3^4\Delta(1)_G$	CASSCF	1299.96590	1.827	28.9	659.6	2.57	3.76	1.23	−0.11	29.0
	MRCI	1300.23941	1.764	56.7	772.8	3.70	3.59	1.11	−0.02	34.4
	MRCI+Q	1300.2601	1.763	61						34
$3^4\Delta(1)_L$	CASSCF	1299.94180	2.461	13.8	275.9				0.12	44.1
	MRCI	1300.18574	2.264	23.0	334.6				0.13	68.1
	MRCI+Q	1300.2031	2.229	25						69
$4^4\Pi(1)$	$CASSCF_G$	1299.94672	2.367	16.2	278.4	3.37	3.63	1.46	0.13	41.1
	$CASSCF_L$	1299.93905	1.767	11.4	510.1	−0.33	9.99	2.51	−0.13	45.9
	MRCI	1300.22810	1.669	49.5	765.9	2.28	5.17	1.57	−0.04	41.5
	MRCI+Q	1300.2528	1.658	56						38
$5^2\Pi(1)$	CASSCF	1299.94612	1.844	45.97	588.3	1.11	2.73	1.46	−0.16	41.4
	MRCI	1300.22355	1.740	56.6	717.2	2.45	3.20	1.39	−0.06	44.4
	MRCI+Q	1300.2456	1.733	59						43
$6^6\Sigma^-(1)$	CASSCF	1299.94560	1.913	16.2	566.5	12.4	6.91	1.27	−0.09	41.8
	MRCI	1300.21216	1.852	39.7	662.9	7.85	5.29	1.13	−0.04	51.5
	MRCI+Q	1300.2334	1.847	44						50
$7^4\Phi(1)$	CASSCF	1299.94696	2.355	16.4	275.9	3.44	3.37	1.53	0.13	40.9
	MRCI	1300.20746	1.826	36.5	607.2	23.9	8.84	1.47	0.09	54.5
	MRCI+Q	1300.2307	1.818	42						52
$8^6\Delta(1)$	$CASSCF_G$	1299.93836	1.945	12.5	605.9	6.16	5.09	1.00	−0.17	46.3
	$CASSCF_L$	1299.93461	2.474	10.2	253.1	6.66	4.83	1.35	0.12	48.7
	MRCI	1300.20482	1.888	35.2	716.8	4.46	3.88	0.85	−0.09	56.1
	MRCI+Q	1300.2258	1.889	39						55
$9^6\Pi(1)_G$	CASSCF	1299.93258	1.913	7.37	530.4	9.03	5.44	1.44	−0.14	49.9
	MRCI	1300.20392	1.811	34.3	724.1	10.1	4.97	1.07	−0.05	56.7
	MRCI+Q	1300.2257	1.808	39						55
	DFT/BPW91[e]		1.80		672					54.9
$9^6\Pi(1)_L$	CASSCF	1299.93908	2.468	11.5	263.8	4.61	5.11	1.26	0.13	45.9
	MRCI	1300.18287	2.243	21.1	345.6	10.3	0.80	1.31	0.13	69.9
	MRCI+Q	1300.2010	2.204	24						71
$10^4\Sigma^-(2)$	MRCI	1300.20330	1.858	34.5	765.2	28.1	8.76	0.81	0.03	57.1
	MRCI+Q	1300.2247	1.857	39						56
$11^4\Pi(2)$	MRCI	1300.20311	1.849	34.2	550.0	14.3	9.83	1.66	0.08	57.2
	MRCI+Q	1300.2257	1.830	39						55
$12^2\Gamma(1)$	MRCI	1300.19345	1.627	38.5	890.3	3.1	4.8	1.4	0.16	63.3
	MRCI+Q	1300.2142	1.630	39						62
$13^4\Delta(2)_G$	MRCI	1300.18937	1.727	26.1	771.5	3.66	5.29	1.26	0.02	65.8
	MRCI+Q	1300.2136	1.728	32						63
$13^4\Delta(2)_L$	MRCI	1300.18563	2.237	23.8					0.12	68.2
	MRCI+Q	1300.2036	2.15	26						69
$14^2\Sigma^+(1)$	MRCI	1300.18857	1.645	35.5	893.6	7.0	3.8	1.3	0.14	66.3
	MRCI+Q	1300.2109	1.647	37						64
$15^6\Delta(2)$	MRCI	1300.18484	1.92	23					0.03	68.7
	MRCI+Q	1300.2077	1.87	28						66
$16^4\Pi(3)$	MRCI	1300.18457	2.073	22.9	~800				0.11	68.8
	MRCI+Q	1300.2047	2.037	26						68

TABLE 2: Continued

state[a]	methods[b,c]	$-E$	r_e	D_e	ω_e	$\omega_e x_e$	$\alpha_e\,(10^{-3})$	$\bar{D}_e\,(10^{-6})$	q_{Fe}	T_e
$17^4\Sigma^+(1)_G$	MRCI	1300.18453	2.274	22.4	304.3	8.59	15.4	1.59	0.12	68.9
	MRCI+Q	1300.2026	2.235	25						70
$17^4\Sigma^+(1)_L$	MRCI	1300.17503	1.785	16.5					−0.03	74.8
	MRCI+Q	1300.2015	1.787	24						70
$18^8\Pi(1)_G$	MRCI	1300.18306	1.992	21.2	578.2	6.79	4.85	0.95	−0.15	69.8
	MRCI+Q	1300.2012	1.991	24.0						71
$18^8\Pi(1)_L$	MRCI	1300.15661	2.871	4.84	122.0	4.02	6.31	2.39	0.10	86.4
	MRCI+Q	1300.1714	2.848	5.26						89
$19^6\Phi(1)$	MRCI	1300.18280	2.244	21.0	344.1	3.95	2.99	1.31	0.13	70.0
	MRCI+Q	1300.2009	2.206	24						71
$20^6\Sigma^+(1)$	MRCI	1300.18235	2.171	21.13	301.1	9.69			0.10	70.2
	MRCI+Q	1300.2019	2.160	24						70
$21^6\Pi(2)_G$	MRCI	1300.18199	2.117	21.0					−0.03	70.5
	MRCI+Q	1300.2031	2.119	25						69
$21^6\Pi(2)_L$	MRCI	1300.17368	2.323	15.8					0.12	75.7
	MRCI+Q	1300.1917	2.275	18						77
$22^4\Gamma(1)$	MRCI	1300.17994	1.775	20.2	820.7	7.24	2.10	0.952	−0.04	71.8
	MRCI+Q	1300.2071	1.780	28						67
$23^2\Phi(1)$	MRCI	1300.17738	1.815	29	594.2	11.5	6.61	1.58	0.18	73.4
	MRCI+Q	1300.2005	1.821	30						71
$24^2\Delta(2)$	MRCI	1300.17664	1.696	28.0	821.3	6.1	3.4	1.2	0.13	73.8
	MRCI+Q	1300.1988	1.702	29						72
$25^8\Sigma^-(1)$	MRCI	1300.17649	2.037	17.1	528.8	8.06	5.48	0.997	−0.15	73.9
	MRCI+Q	1300.1945	2.032	20						75
$26^8\Delta(1)_G$	MRCI	1300.17568	2.023	16.9	575.9	9.63	5.76	0.873	−0.13	74.4
	MRCI+Q	1300.1968	2.017	21						73
$26^8\Delta(1)_L$	MRCI	1300.15538	2.933	4.19	105.1	5.97	5.20	2.86	0.08	87.2
	MRCI+Q	1300.1703	2.877	4.6						90
$27^2\Pi(2)$	MRCI	1300.17476	1.820	27	528.8	1.79	1.08	1.96	0.17	75.0
	MRCI+Q	1300.1980	1.825	29						73
$28^6\Pi(3)_G$	MRCI	1300.17215	2.207	15.1					0.06	76.6
	MRCI+Q	1300.1919	2.220	18						76
$28^6\Pi(3)_L$	MRCI	1300.15866	1.833	6.68					−0.07	85.1
	MRCI+Q	1300.1838	1.835	13.4						81
$29^2H(1)$	MRCI	1300.16868	1.641	65.5	830.9	2.88	4.97	1.48	0.00	78.8
	MRCI+Q	1300.1918	1.638	68						76
$30^2\Pi(3)$	MRCI	1300.16800	1.707	23	1054.1	23.6	7.08	7.21	0.06	79.2
	MRCI+Q	1300.1928	1.709	25						76
$31^2\Phi(2)$	MRCI	1300.16381	1.655	20	807.9	5.22	3.22	1.49	0.01	81.9
	MRCI+Q	1300.1874	1.653	22						79
$32^6\Gamma(1)$	MRCI	1300.16181	1.901	17.7	677.3	2.50	2.26	0.918	0.02	83.1
	MRCI+Q	1300.1881	1.911	22						79
$33^6\Sigma^+(2)$	MRCI	1300.15706	1.971	14.7	681.6	12.9	2.23	0.738	0.05	86.1
	MRCI+Q	1300.1830	1.979	19						82
$34^8\Phi(1)$	MRCI	1300.15652	2.875	4.82	121.6	2.99	6.10	2.38	0.10	86.4
	MRCI+Q	1300.1712	2.852	5.2						89
$35^8\Pi(2)_G$	MRCI	1300.15592	2.647	4.60	482				0.14	86.8
	MRCI+Q	1300.1711	2.680	5.1						89
$35^8\Pi(2)_L$	MRCI	1300.15435	3.089	3.61	96.1	1.82	4.85	2.47	0.07	87.8
	MRCI+Q	1300.1693	3.039	3.9						91
$36^8\Sigma^+(1)$	MRCI	1300.15503	2.987	3.97	104.0	1.93	5.43	2.59	0.08	87.4
	MRCI+Q	1300.1699	2.946	4.4						90
$37^8\Delta(2)$	MRCI	1300.15381	2.630	3.38	435				0.09	88.1
	MRCI+Q	1300.1699	2.668	4.5						90
$38^8\Pi(3)$	MRCI	1300.15348	2.782	2.63	419	50			0.06	88.4
	MRCI+Q	1300.1686	2.780	3.6						91
$39^6\Delta(3)$	MRCI	1300.15103	2.020	10.9	761.3	1.84	0.734	0.505	0.10	89.9
	MRCI+Q	1300.1760	2.022	15						86

[a] Numbers in parentheses refer to the ordering of states within the same symmetry manifold; G and L subscripts refer to global and local minima. [b] Internally contracted MRCI. [c] +Q, +DKH, and +CG refer to the multireference Davidson correction and scalar relativistic corrections via the Douglas−Kroll−Hess and Cowan−Griffin approaches, respectively. [d] The semicore $3s^23p^6$ of Fe^+ is included in the CI procedure. [e] Reference 8. [f] Reference 5, D_0 value. [g] Reference 6, D_0 value.

Finally, for the ionization potential of the FeC molecule, we obtain 6.81 (7.10) [7.38] eV at the C-MRCI (C-MRCI+Q) [C-RCCSD(T)] levels of theory, as compared with the experimental value of 7.74 ± 0.09 eV.[16]

$2^2\Sigma^-$(1). This is the second excited state of FeC^+, located 27.8 (28) kcal/mol above the $X^2\Delta$ state at the MRCI (MRCI+Q) level. It is a truly multireference state, as can been seen from the most important CASSCF equilibrium CFs:

$$|2^2\Sigma^-\rangle_{A_2} \sim |1\sigma^2 2\sigma^2 3\sigma^1 1\pi_x^2 1\pi_y^2[0.67(1\bar{\delta}_+^1 1\delta_-^1) + 0.39 (1\delta_+^1 1\bar{\delta}_-^1)]\rangle + |1\sigma^2 2\sigma^2 3\sigma^1[0.20(1\bar{\pi}_x^1 2\bar{\pi}_x^1 1\pi_y^2 + 1\pi_x^2 1\bar{\pi}_y^1 2\bar{\pi}_y^1)1\delta_+^1 1\delta_-^1 - 0.19(1\pi_x^2 1\pi_y^1 2\pi_y^1 + 1\pi_x^1 2\pi_x^1 1\pi_y^2)1\bar{\delta}_+^1 1\bar{\delta}_-^1 - 0.18(1\pi_x^2 2\pi_y^2 + 2\pi_x^2 1\pi_y^2)1\bar{\delta}_+^1 1\delta_-^1]\rangle$$

At infinity, it correlates to $|^4F;\ M = \pm 1\rangle_{Fe} \times |^3P;\ M = \mp 1\rangle_C$, maintaining this character up to equilibrium. Despite its mul-

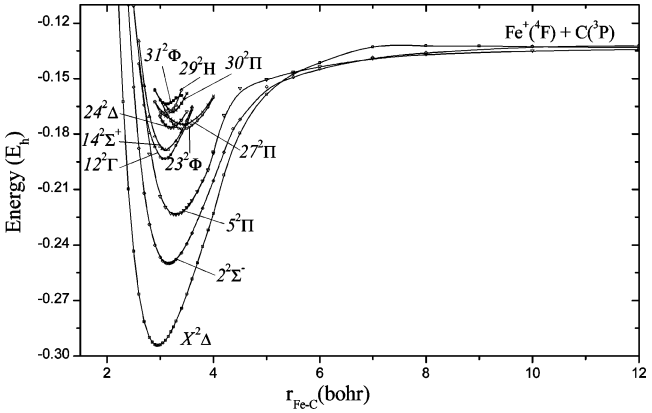

Figure 3. MRCI PECs of the doublet states of the FeC^+ cation.

tireference description, we can attempt a graphical representation of the bonding:

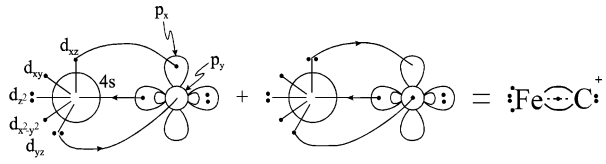

The following CASSCF atomic populations indicate a charge migration from Fe^+ to C via the π system and from C to Fe^+ through the σ system, in agreement with the qualitative picture above.

$$4s^{0.66}4p_z^{0.07}3d_{z^2}^{1.69}3d_{xz}^{1.29}4p_x^{0.03}3d_{yz}^{1.29}4p_y^{0.03}3d_{x^2-y^2}^{1.00}3d_{xy}^{1.00}/$$
$$2s^{1.71}2p_z^{0.83}2p_x^{0.64}2p_y^{0.64}$$

D_e = 73.1 kcal/mol and r_e = 1.670 Å at the MRCI level, reflecting the loss of a $^1/_2\sigma$ bond relative to the $X^2\Delta$ state; see Figure 3 for the PEC of this state.

$5^2\Pi(1)$. This state correlates to $Fe^+(^4F;\ M = \pm2) + C(^3P;\ M = \mp1)$, but near 4.5 bohr an avoided crossing with the $27^2\Pi$-(2) state changes its equilibrium character to $Fe^+(^4F;\ M = \pm1) + C(^3P;\ M = 0)$. As in the $2^2\Sigma^-(1)$ case, the CASSCF equilibrium vector spreads thin among many CFs, a sample of which up to $\sum_i|C_i|^2 \cong 0.6$ is given below.

$$|5^2\Pi(1)\rangle_{B_1} \sim |1\sigma^2 2\sigma^2 1\delta_+^1[0.50(1\pi_x^2 1\pi_y^2 2\bar{\pi}_y^1 1\delta_-^1) -$$
$$0.32(1\pi_x^1 2\bar{\pi}_x^1 1\pi_y^2 2\bar{\pi}_y^1 1\delta_-^1) - 0.29(1\pi_x^2 1\pi_y^2 2\pi_y^1 1\bar{\delta}_-^1)]\rangle +$$
$$|[0.23(1\sigma^2 3\sigma^2 1\delta_+^1 1\delta_-^1) - 0.20(1\sigma^2 2\sigma^1 3\sigma^1 1\delta_+^1 1\bar{\delta}_-^1) -$$
$$0.19(1\sigma^2 2\sigma^1 3\sigma^1 1\bar{\delta}_+^1 1\delta_-^1)](1\pi_x^2 1\pi_y^2 2\bar{\pi}_y^1)\rangle$$

Taking into consideration the configurations as well the CASSCF Mulliken atomic distributions (Fe^+/C),

$$4s^{0.31}4p_z^{0.12}3d_{z^2}^{1.13}3d_{xz}^{1.20}4p_x^{0.03}3d_{yz}^{1.99}4p_y^{0.04}3d_{x^2-y^2}^{1.01}3d_{xy}^{1.01}/$$
$$2s^{1.62}2p_z^{0.81}2p_x^{0.77}2p_y^{0.95}$$

the bonding can be grasped qualitatively by the icon featuring a 0.4 e^- donation from $Fe^+(4s4p_z3d_{z^2})^{2.0}$ to the empty $2p_\sigma$ C orbital and a back-transfer of about 0.25 e^- to the Fe^+ species through the π system. At the MRCI (MRCI+Q) levels, D_e = 56.6 (59) kcal/mol and r_e = 1.740 (1.733) Å, respectively; see Table 2.

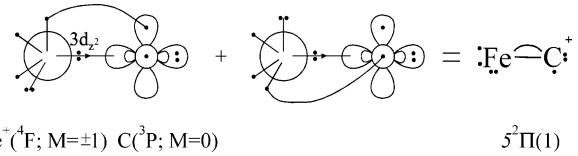

$12^2\Gamma(1)$. This state correlates to $Fe^+(^4F;\ M = \pm3) + C(^3P;\ M = \pm1)$, carrying this character down to the equilibrium bond distance. The dominant equilibrium CASSCF CFs, considering both spatial symmetries ($A_1 + A_2$) and the atomic populations, are

$$|12^2\Gamma(1)\rangle_{A_1+A_2} \sim 1/\sqrt{2}|1\sigma^2 2\sigma^2 3\sigma^1 1\pi_x^2 1\pi_y^2[0.62(1\delta_+^2 +$$
$$1\delta_-^2) + 0.76(1\delta_+^1 1\bar{\delta}_-^1) + 0.44(1\bar{\delta}_+^1 1\delta_-^1)]\rangle$$
$$4s^{0.58}4p_z^{0.08}3d_{z^2}^{1.64}3d_{xz}^{1.38}4p_x^{0.02}3d_{yz}^{1.38}4p_y^{0.02}3d_{x^2-y^2}^{1.01}3d_{xy}^{1.01}/$$
$$2s^{1.75}2p_z^{0.91}2p_x^{0.59}2p_y^{0.59}$$

About 0.35 e^- are donated from the C $2p_\sigma$ orbital to the empty 4s orbital of Fe^+, resulting in a $^1/_2\sigma$ bond, with a concomitant transfer of 0.20 e^- from Fe^+ to C via the π skeleton. The bonding can be described graphically by the vbL icons below suggesting 2 π and $^1/_2$ σ bonds.

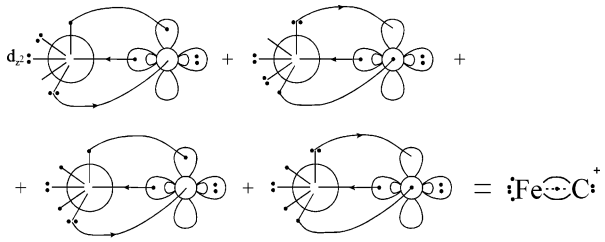

The MRCI (MRCI+Q) interaction energy (D_e) and bond length (r_e) are 38.5 (39) kcal/mol and 1.627 (1.630), respectively. This state of FeC^+ is completely analogous to the $34^3\Gamma(1)$ state of (neutral) FeC; the latter state has a MRCI[2,17] binding energy and bond length of 28 kcal/mol and 1.79 Å but with 1 σ and $^1/_2$ π bond character.[2]

29^2H(1). This state correlates adiabatically to $Fe^+(d^7,\ ^2G;\ M = \pm4)$, the fourth excited state of $Fe^+ + C(^3P;\ M = \pm1)$. However, an avoided crossing with a higher $^2H(2)$ state stemming from the a^2H atomic state of Fe^+ imparts its character to the in situ equilibrium atoms, $Fe^+(d^7,\ ^2H;\ M = \pm5$; sixth excited state of $Fe^+) + C(^3P;\ M = 0)$. The leading CASSCF CFs and Mulliken atomic distributions (Fe^+/C)

$$|29^2H(1)\rangle_{B_1} \sim |1\sigma^2 2\sigma^2 1\delta^1{}_+ 1\pi_x^2 1\pi_y^2[0.52(2\pi_y^1 1\bar{\delta}_-^1) +$$
$$0.30(2\bar{\pi}_y^1 1\delta_-^1)] - 0.43|1\sigma^2 2\sigma^2 1\pi_x^2 2\pi_x^1 1\pi_y^2(1\delta_+^2 - 1\delta_-^2)\rangle$$
$$4s^{0.19}4p_z^{0.11}3d_{z^2}^{1.33}3d_{xz}^{1.61}4p_x^{0.04}3d_{yz}^{1.61}4p_y^{0.04}3d_{x^2-y^2}^{1.00}3d_{xy}^{1.00}/$$
$$2s^{1.69}2p_z^{0.65}2p_x^{0.84}2p_y^{0.84}$$

are pointing to a $\sigma^2\pi^2$ bonding scheme. The $2p_\sigma$ C orbital accepts 0.34 e^- from the $(4s4p_z3d_{z^2})^{2.0}$ Fe^+ hybrid, while an equal charge transfer is observed from C to Fe^+ along the π system. The bonding can be visualized by the following vbL abstractions.

The MRCI (MRCI+Q) adiabatic dissociation energies, D_e, are 65.5 (68) kcal/mol at r_e = 1.641 (1.638) Å, but the intrinsic bond strengths, i.e., with respect to $Fe^+(^2H) + C(^3P)$, amount to 65.5 (68) + $\Delta E(^2H \leftarrow {}^2G)$ = 78.3 (81) kcal/mol. The $29^2H(1)$

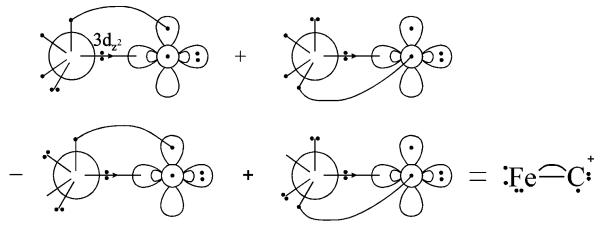

state is analogous to the 35^1H(1) state of the neutral FeC[Fe($4s^23d^6$, ^{3}H; M = ±5) + C(^{3}P; M = 0)], with D_e and r_e MRCI values of 65 kcal/mol and 1.675 Å, respectively;[2,17] see Figure 1.

B. Quartets. All 10 quartets, but the $22^4\Gamma(1)$, trace their lineage to the ground-state atoms, $Fe^+(^6D) + C(^3P)$; see Figure 4.

$1^4\Sigma^-(1)$. This is the lowest of the quartets and the first excited ($a^4\Sigma^-$) state of FeC^+, located 19.0 (18) kcal/mol above the $X^2\Delta$ state at the MRCI (MRCI+Q) level of theory, tracing its ancestry to $Fe^+(^6D; M = \pm1) + C(^3P; M = \mp1)$. Its main CASSCF equilibrium configuration $|1^4\Sigma^-\rangle \cong 0.82|1\sigma^2 2\sigma^2 3\sigma^1 1\pi_x^2 1\pi_y^2 1\delta_+^1 1\delta_-^1\rangle$ and Mulliken atomic populations are

$$4s^{0.74}4p_z^{0.07}3d_{z^2}^{1.43}3d_{xz}^{1.40}4p_x^{0.02}3d_{yz}^{1.40}4p_y^{0.02}3d_{x^2-y^2}^{1.00}3d_{xy}^{1.00}/ 2s^{1.83}2p_z^{0.90}2p_x^{0.57}2p_y^{0.57}$$

Through the π skeleton, the C atom gains about 0.14 e^-, but 0.27 e^- migrate from the $2p_z$ singly occupied orbital of C to a $\sim(4s3d_{z^2}2p_z)$ hybrid on Fe^+. The resulting triple-bonded molecule is clearly represented by the diagram:

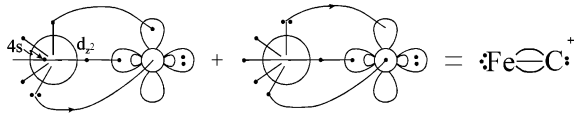

The MRCI (MRCI+Q) D_e and r_e values are 72.2 (76) kcal/mol and 1.667 (1.671) Å, respectively, 28.6 (25) kcal/mol smaller and 0.104 (0.103) Å larger than the D_e and r_e values of the similarly bonded $X^2\Delta$ state. At the DFT level, Gutsev and Bauschlicher[8] reported $r_e = 1.64$ Å, $\omega_e = 831$ cm^{-1}, and $T_e(1^4\Sigma^- \leftarrow X^2\Delta) = 16.6$ kcal/mol, in relatively good agreement with our MRCI results.

$3^4\Delta(1)$. This state is located 15.4 kcal/mol above the $1^4\Sigma^-(1)$, correlating to $|^6D; M = \pm1\rangle_{Fe} \times |^3P; M = \pm1\rangle_C$. However, the result of an avoided crossing at 4.2 bohr (Figure 4) with the $13^4\Delta(2)$ state changes the in situ character of the metal atom to $Fe^+(^4F; M = \mp3 \text{ or } \pm1)$. The following are the first five main configurations with $\sum_i|C_i|^2 \cong 0.7$, showing its intense multireference character.

$$|3^4\Delta(1)\rangle_{A_1} \sim |\{(1\sigma^2 2\sigma^1 3\sigma^1)[0.57(1\pi_x^2 1\pi_y^2) - 0.21(1\pi_x^2 2\pi_y^2 + 2\pi_x^2 1\pi_y^2)] - 0.36(1\sigma^2 2\sigma^2)(1\pi_x^1 2\pi_x^1 1\pi_y^2 + 1\pi_x^2 1\pi_y^1 2\pi_y^1)\}1\delta_+^1 1\delta_-^2\rangle$$

The CASSCF Mulliken atomic populations

$$4s^{0.34}4p_z^{0.11}3d_{z^2}^{1.09}3d_{xz}^{1.15}4p_x^{0.03}3d_{yz}^{1.15}4p_y^{0.03}3d_{x^2-y^2}^{1.00}3d_{xy}^{2.00}/ 2s^{1.63}2p_z^{0.82}2p_x^{0.82}2p_y^{0.82}$$

in conjunction with the symmetry of the atoms at equilibrium,

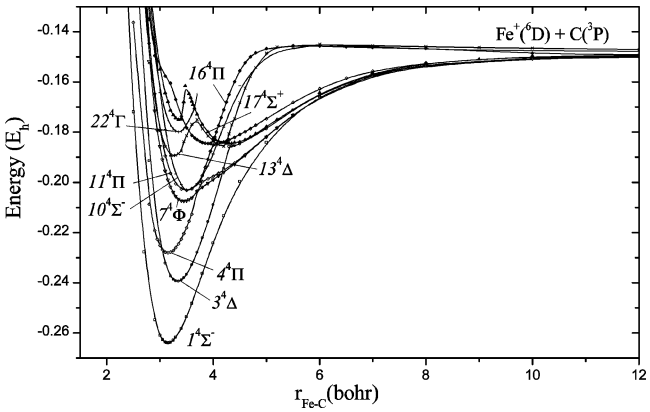

Figure 4. MRCI PECs of the quartet states of the FeC^+ cation.

suggest 2 π and $^1/_2$ σ bonds and a total transfer of 0.1 e^- from Fe^+ to C. Graphically,

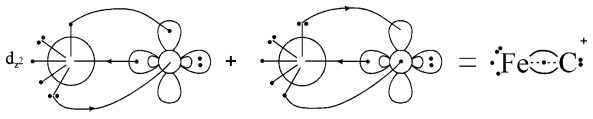

With respect to the adiabatic fragments, the MRCI (MRCI+Q) D_e and r_e values are 56.7 (61) kcal/mol and 1.764 (1.763) Å, whereas diabatically, $D_e = 66.4$ (68) kcal/mol.

$13^4\Delta(2)$. This state, Figure 4, correlates to $Fe^+(^6D; M = \pm2) + C(^3P, M = 0)$. It features three avoided crossings, one with the $^4\Delta(3)$ state (which has not been calculated) correlating to $Fe^+(^4F; M = \pm3 \text{ or } \mp1) + C(^3P, M = \mp1)$ around 4.4 bohr, the second at 4.2 bohr with the $3^4\Delta(1)$ state (vide supra) thus acquiring the character $Fe^+(^6D; M = \pm1) + C(^3P, M = \pm1)$, and finally, the third one occurring at 3.7 bohr with the $^4\Delta(3)$ state, again having the character $Fe^+(^4F; M = \mp3 \text{ or } \pm1) + C(^3P, M = \pm1)$. The two minima, global (G) and local (L) at 1.727 and 2.237 Å, respectively, are connected through a barrier of 9.0 kcal/mol with respect to the G minimum.

$4^4\Pi(1)$. The asymptotic fragments of $4^4\Pi(1)$ are $Fe^+(^6D; M = \pm2) + C(^3P; M = \mp1)$. Because of an avoided crossing around 3.75 bohr with the $11^4\Pi(2)$ state, which has already suffered an avoided crossing with the $16^4\Pi(3)$ state, the in situ atoms carry the memory of the $16^4\Pi(3)$ state, i.e., $Fe^+(^4F; M = \pm1) + C(^3P; M = 0)$, Figure 4. However, it should be observed that the character of the $16^4\Pi(3)$ state is the result of an avoided crossing with a (not calculated) $^4\Pi(4)$ state correlating, of course, to $Fe^+(^4F; M = \pm1) + C(^3P; M = 0)$. The leading MRCI CFs in conjunction with the Mulliken densities

$$|4^4\Pi(1)\rangle_{B_1+B_2} \sim 0.77/\sqrt{2}|1\sigma^2 2\sigma^2(1\pi_x^2 1\pi_y^2 2\pi_y^1 + 1\pi_x^2 2\pi_x^1 1\pi_y^2)1\delta_+^1 1\delta_-^1\rangle$$

$$4s^{0.22}4p_z^{0.07}3d_{z^2}^{1.31}3d_{xz}^{1.40}4p_x^{0.02}3d_{yz}^{1.78}4p_y^{0.08}3d_{x^2-y^2}^{1.01}3d_{xy}^{1.01}/ 2s^{1.68}2p_z^{0.66}2p_x^{0.55}2p_y^{1.07}$$

point to a $\sigma^2\pi^2$ bonding scheme, shown graphically below.

The bonding is the result of a 0.3 e^- transfer from Fe^+ to C via the σ frame and from C to Fe^+ through the π system. With MRCI D_e and r_e values of 49.5 kcal/mol and 1.669 Å and with analogous types of avoided crossings, the $4^4\Pi(1)$ state is closely related to the $3^5\Pi(1)$ state of FeC ($D_e = 57$ kcal/mol, $r_e = 1.68$

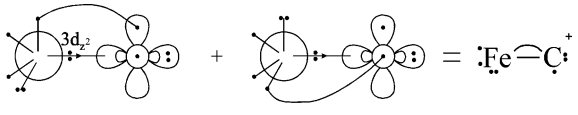

$Fe^+(^4F; M=\pm1)$ $C(^3P; M=0)$ $4^4\Pi(1)$

Å).[2,17] The latter state is obtained by attaching an electron to the empty 4s Fe orbital of the $4^4\Pi(1)$ state coupled into a quintet.

$11^4\Pi$(2) and $16^4\Pi$(3). These states, shown in Figure 4, are similar to the $17^5\Pi(2)$ and $24^5\Pi(3)$ states of neutral FeC, respectively, but with different in situ character, $Fe^+(^6D; M = \pm2, 0) + C(^3P; M = \mp1)$.[2]

$7^4\Phi$ (1). Two of the most important MRCI equilibrium configurations of $7^4\Phi$ (B_1 symmetry) are

$$|1\sigma^2 2\sigma^2 3\sigma^1[(0.55)1\pi_x^2 1\pi_y^1 1\delta_+^2 1\delta_-^1 + (0.52)1\pi_x^1 1\pi_y^2 1\delta_+^1 1\delta_-^2]\rangle$$

Asymptotically, this state correlates to $Fe^+(^6D; M = \pm2) + C(^3P; M = \pm1)$ and maintains this character up to $r_e = 1.826$ Å. The equilibrium MRCI populations

$$4s^{0.55}4p_z^{0.07}3d_{z^2}^{1.29}3d_{xz}^{1.08}4p_x^{0.02}3d_{yz}^{1.06}4p_y^{0.02}3d_{x^2-y^2}^{1.52}3d_{xy}^{1.46}/$$
$$2s^{1.83}2p_z^{1.13}2p_x^{0.46}2p_y^{0.43}$$

imply the following bonding diagram, indicating a $^3/_2$ π and 1 σ bonding structure.

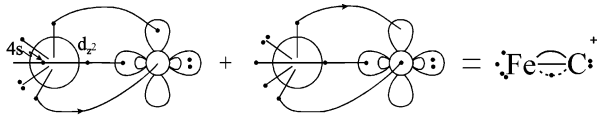

$Fe^+(^6D; M=\pm2)$ $C(^3P; M=\pm1)$ $7^4\Phi(1)$

A $4s3d_{z^2}$ hybrid orbital on Fe^+ interacting with the $2p_z$ C orbital is the cause of the σ bond; the total charge on the metal is less than +1, indicating a small electron transfer from C to Fe^+ through the π system.

The analogous $26^5\Phi(1)$ PEC of the neutral FeC shows two minima, a local (L) and a global (G).[2] The L-isomer has a similar bonding interaction with the $7^4\Phi(1)$ of FeC^+ but with D_e and r_e values of 16 kcal/mol and 2.02 Å,[2] as contrasted to 36.5 kcal/mol and 1.826 Å of FeC^+. In the G-minimum of the $26^5\Phi(1)$ state, the Fe atom is excited, with $D_e = 19$ kcal/mol and $r_e = 1.69$ Å.[2,17]

It is also interesting that, at the CASSCF level, both the $3^4\Pi$-(1) (before crossing) and $7^4\Phi(1)$ states present a global minimum around 4.5 bohr. The σ bond is of $4s_{Fe^+}-2p_{z/C}$ origin, but around 3.4 bohr (MRCI minimum), the σ bond changes character, becoming $3d_\sigma-2p_z$ and resulting in a higher bond strength.

C. Sextets. The PECs of the 11 sextets presently studied are displayed in Figure 5; six of these states will be described in some detail in the following. With the exception of the $32^6\Gamma$ and $39^6\Delta$ states, which correlate to $Fe^+(^4F) + C(^3P)$, the sextets trace their end fragments to the ground-state atoms, $Fe^+(^6D) + C(^3P)$.

$6^6\Sigma^-$(1). The lowest of the sextets is of the Σ^- spatial symmetry $6^6\Sigma^-(1)$, a strongly multireference state whose CASSCF leading CFs are

$$|6^6\Sigma^-(1)\rangle_{A_2} \sim |(1\sigma^2 2\sigma^2 3\sigma^1)\{0.57(1\pi_x^1 2\pi_x^1 1\pi_y^2 + 1\pi_x^2 1\pi_y^1 2\pi_y^1)1\delta_+^1 1\delta_-^1 - (1\pi_x^1 2\pi_x^1 1\pi_y^1 2\pi_y^1)[0.27(1\bar\delta_+^1 1\delta_-^1) + 0.22(1\delta_+^1 1\bar\delta_-^1)] - 0.21(2\pi_x^2 1\pi_y^1 2\pi_y^1 + 1\pi_x^1 2\pi_x^1 2\pi_y^2)1\delta_+^1 1\delta_-^1\}\rangle$$

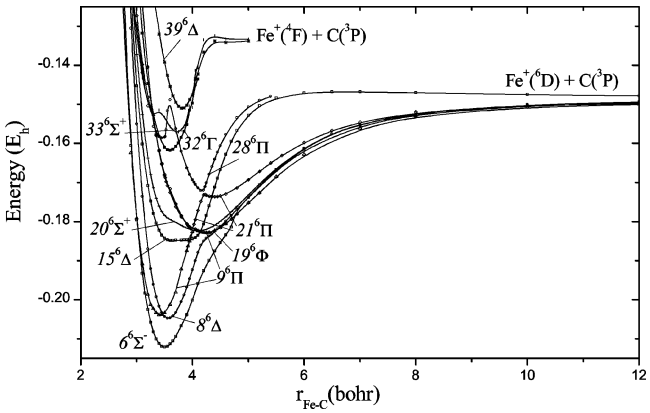

Figure 5. MRCI PECs of the sextet states of the FeC^+ cation.

An avoided crossing around 4.3 bohr with an incoming $^6\Sigma^-(2)$ state changes its equilibrium character from its asymptote, $Fe^+(^6D; M = \pm1) + C(^3P; M = \mp1)$, to the corresponding M = (0, 0) component. At $r_e = 1.852$ Å, we calculate a D_e of 39.7 kcal/mol, whereas the Mulliken distributions

$$4s^{0.66}4p_z^{0.07}3d_{z^2}^{1.78}3d_{xz}^{1.15}4p_x^{0.04}3d_{yz}^{1.15}4p_y^{0.04}3d_{x^2-y^2}^{1.00}3d_{xy}^{1.00}/$$
$$2s^{1.75}2p_z^{0.72}2p_x^{0.80}2p_y^{0.80}$$

indicate the formation of a $^1/_2$ σ and a π bond, the result of about a 0.5 e^- current moving from Fe^+ to C via the σ frame and a back-current of 0.4 e^- returning to Fe^+ through the π frame. Graphically,

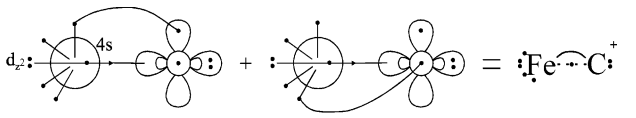

$Fe^+(^6D; M=0)$ $C(^3P; M=0)$ $6^6\Sigma^-(1)$

$8^6\Delta$(1). The next sextet, located 4.6 kcal/mol higher, is a $8^6\Delta$-(1) state comprising the following main CASSCF CFs:

$$|8^6\Delta(1)\rangle_{A_1} \sim |(1\sigma^2 2\sigma^1 3\sigma^1 1\delta_+^1 1\delta_-^2)[0.42(1\pi_x^1 2\pi_x^1 1\pi_y^2 + 1\pi_x^2 1\pi_y^1 2\pi_y^1) + 0.40(1\pi_x^1 2\bar\pi_x^1 1\pi_y^1 2\pi_y^1) + 0.37(1\pi_x^1 2\pi_x^1 1\pi_y^1 2\bar\pi_y^1)]\rangle + |[0.31(1\sigma^2 2\sigma^1 3\sigma^1 1\bar\delta_+^1 1\delta_-^2) + 0.26(1\sigma^2 2\sigma^2 1\delta_+^1 1\delta_-^2)](1\pi_x^1 2\pi_x^1 1\pi_y^1 2\pi_y^1)\rangle$$

Adiabatically, it relates to the end products $Fe^+(^6D; M = \pm1) + C(^3P; M = \pm1)$. At 4.2 bohr, it suffers an avoided crossing with the $15^6\Delta(2)$ state, thus, at equilibrium, acquires the character of the $15^6\Delta(2)$ state, $Fe^+(^6D; M = \pm2) + C(^3P; M = 0)$; see Figure 5. At $r_e = 1.888$ Å and $D_e = 35.2$ kcal/mol, the attractive interaction, being the result of $^1/_2$ σ and a π bond, is represented schematically by the following vbL diagrams

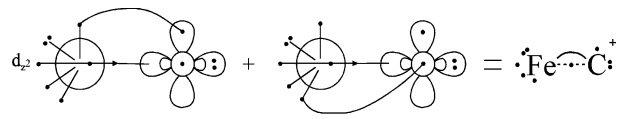

$Fe^+(^6D; M=\pm2)$ $C(^3P; M=0)$ $8^6\Delta(1)$

and is corroborated from the Mulliken CASSCF atomic populations

$$4s^{0.52}4p_z^{0.06}3d_{z^2}^{1.04}3d_{xz}^{1.07}4p_x^{0.03}3d_{yz}^{1.07}4p_y^{0.03}3d_{x^2-y^2}^{1.00}3d_{xy}^{1.00}/\ 2s^{1.64}2p_z^{0.72}2p_x^{0.89}2p_y^{0.89}$$

The bonding is identical to that of the previously described $6^6\Sigma^-(1)$ sextet state.

$9^6\Pi(1)$. This state shows an interesting topology: adiabatically, it correlates to $Fe^+(^6D;\ M = \pm2) + C(^3P;\ M = \mp1)$, whereas up to 4.05 bohr, its PEC is identical to that of the $19^6\Phi(1)$ state, Figure 5. At this point, an avoided crossing occurs with the $21^6\Pi(2)$ state, which has already suffered an avoided crossing with the $28^6\Pi(3)$ state. Therefore, the latter imparts its character to the global minimum of the $9^6\Pi(1)$ state, i.e., $Fe^+(^6D;\ M = \pm1) + C(^3P;\ M = 0)$, with its local minimum coinciding exactly with the minimum of the $19^6\Phi(1)$ state; see Figure 5. We give below the leading CASSCF CFs of the $9^6\Pi(1)_G$ and $9^6\Pi(1)_L$ minima, the latter being identical to that of the $19^6\Phi(1)$ state, apart from a sign change.

$$|9^6\Pi(1)\rangle_{B_1,G} \sim |(1\sigma^2 2\sigma^1 3\sigma^1)[0.58(1\pi_x^2 1\pi_y^2 2\pi_y^1) - 0.43(1\pi_x^1 2\bar{\pi}_x^1 1\pi_y^2 2\pi_y^1) - 0.29(1\pi_x^1 2\pi_x^1 1\pi_y^2 2\bar{\pi}_y^1)]1\delta_+^1 1\delta_-^1\rangle + |[0.31(1\sigma^2 2\sigma^1 3\sigma^1 1\bar{\delta}_+^1 1\delta_-^1) + 0.26(1\sigma^2 2\sigma^1 3\sigma^1 1\delta_+^1 1\bar{\delta}_-^1) - 0.23(1\sigma^2 2\sigma^2 1\delta_+^1 1\delta_-^1)](1\pi_x^1 2\pi_x^1 1\pi_y^2 2\pi_y^1)\rangle$$

$$|9^6\Pi(1)\rangle_{B_1,L}/|19^6\Phi(1)\rangle_{B_1} \sim 0.56|1\sigma^2 2\sigma^2 3\sigma^1 (1\pi_x^1 2\pi_x^1 1\pi_y^1 1\delta_+^2 1\delta_-^1 \mp 1\pi_x^1 1\pi_y^1 2\pi_y^1 1\delta_+^1 1\delta_-^2)\rangle$$

The equilibrium Mulliken distributions of the $9^6\Pi(1)_G$ state

$$4s^{0.57}4p_z^{0.06}3d_{z^2}^{1.03}3d_{xz}^{1.16}4p_x^{0.03}3d_{yz}^{1.96}4p_y^{0.04}3d_{x^2-y^2}^{1.00}3d_{xy}^{1.00}/\ 2s^{1.64}2p_z^{0.69}2p_x^{0.80}2p_y^{0.98}$$

and the symmetry of the in situ atoms support the following self-explanatory bonding diagrams.

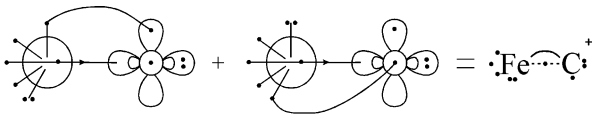

$Fe^+(^6D;\ M=\pm1)$ $C(^3P;\ M=0)$ $9^6\Pi_G(1)$

At the MRCI (MRCI+Q) level, $D_e = 34.3$ (39) kcal/mol and $r_e = 1.811$ (1.808) Å. Note that although, formally, the $8^6\Delta(1)$ state was lower than the $9^6\Pi_G(1)$ state by 0.6 kcal/mol at the MRCI level, with the addition of the Davidson correction this difference becomes practically naught, i.e., the two states are degenerate.

$15^6\Delta(2)$ and $20^6\Sigma^+(1)$. These two sextets correlate to $Fe^+(^6D;\ M = \pm2, \mp1) + C(^3P;\ 0, \mp1)$. The square well-like potential of the $15^6\Delta(2)$, Figure 5, is the result of an avoided crossing with the $8^6\Delta(1)$ state at 4.2 bohr (vide infra) and the character change of the incipient σ bond formation through the participation of the $Fe^{+'}$ 4s orbital but replaced gradually by its $3d_{z^2}$ orbital as we move toward the equilibrium. Certainly, the bond length is ill-defined, an approximate value which corresponds to the middle of the well, being about 2.0 Å. The bonding comprises one σ and one π bond with $D_e \cong 23$ kcal/mol (see below).

The in situ atomic character of the $20^6\Sigma^+(1)$ state is the same as that of the $15^6\Delta(2)$ state, namely, $Fe^+(^6D;\ M = \mp1/\pm1) + C(^3P;\ \pm1)$, with its PEC presenting the same broad morphology around equilibrium as that of the $15^6\Delta(2)$ state and for the same reasons. A minimum can be located around 2.17 Å with $D_e \cong$ 21 kcal/mol.

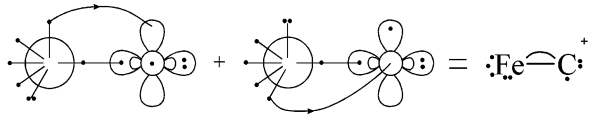

$Fe^+(^6D;\ M=\pm1)$ $C(^3P;\ M=\pm,\mp1)$ $15^6\Delta(2), 20^6\Sigma^+(1)$

D. Octets. Eight octet states have been calculated, all correlating to the ground-state atoms $Fe^+(^6D) + C(^3P)$; Figure 6. We discuss two of them, namely, the $18^8\Pi(1)$ state (the lowest of the octets) and the $25^8\Sigma^-(1)$ state (the first excited state among the octet manifold), 4.2 kcal/mol above the $18^8\Pi(1)$ state.

$18^8\Pi(1)$. This state correlates adiabatically to $Fe^+(^6D;\ M = \pm2) + C(^3P;\ M = \mp1)$; this character is maintained up to the local minimum close to 5.4 bohr. At exactly 5.0 bohr, an avoided crossing occurs with the $35^8\Pi(2)$ state, which has already suffered an avoided crossing with the $38^8\Pi(3)$ state, imparting its character to the in situ atoms of the $18^8\Pi(1)$ state, $Fe^+(^6D;\ M = \pm1) + C(^3P;\ M = 0)$. These interesting topological features are very nicely shown in Figure 6. As is expected, the B_1 (or B_2) component of the $18^8\Pi(1)$ state is completely described at the global minimum by a "single" configuration,

$$0.99/\sqrt{2}|1\sigma^2 2\sigma^1 3\sigma^1(1\pi_x^1 2\pi_x^1 1\pi_y^2 2\pi_y^1 + 1\pi_x^2 2\pi_x^1 1\pi_y^1 2\pi_y^1)1\delta_+^1 1\delta_-^1\rangle_{B_1+B_2}$$

which in conjunction with the Mulliken populations

$$4s^{0.62}4p_z^{0.08}3d_{z^2}^{1.03}3d_{xz}^{1.01}4p_x^{0.04}3d_{yz}^{2.00}4p_y^{0.04}3d_{x^2-y^2}^{1.00}3d_{xy}^{1.00}/\ 2s^{1.64}2p_z^{0.61}2p_x^{0.94}2p_y^{0.95}$$

points clearly to the following bonding icon:

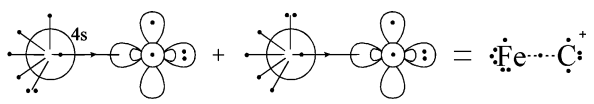

$Fe^+(^6D;\ M=\pm1)$ $C(^3P;\ M=0)$ $18^8\Pi(1)$

With the π route closed to charge transfer, about 0.2 e^- migrate to the empty $2p_z$ C orbital, creating a $^1/_2$ σ bond and giving rise to binding energies of 21.2 (24) kcal/mol and $r_e =$ 1.992 (1.991) Å at the MRCI (MRCI+Q) level.

$25^8\Sigma^-(1)$. This state is also a single reference state whose Hartree−Fock configuration,

$$\sim 0.98|1\sigma^2 2\sigma^2 3\sigma^1 1\pi_x^1 2\pi_x^1 1\pi_y^1 2\pi_y^1 1\delta_+^1 1\delta_-^1\rangle_{A_2}$$

and Mulliken distributions

$$4s^{0.70}4p_z^{0.08}3d_{z^2}^{1.97}3d_{xz}^{1.01}4p_x^{0.04}3d_{yz}^{1.01}4p_y^{0.04}3d_{x^2-y^2}^{1}3d_{xy}^{1}/\ 2s^{1.70}2p_z^{0.54}2p_x^{0.95}2p_y^{0.95}$$

lead, similarly, to the previously described state, i.e., a $^1/_2$ σ bond and a charge transfer of about 0.2 e^- from Fe^+ to the empty $2p_z$ C orbital. With respect to the adiabatic products $Fe^+(^6D;\ M = 0) + C(^3P;\ M = 0)$, the MRCI (MRCI+Q) binding energies (D_e) are 17.1 (20) kcal/mol at $r_e = 2.037$ (2.032) Å; see Figure 6 and Table 2.

$26^8\Delta(1)$ and $37\ ^8\Delta(2)$. These states correlate to $Fe^+(^6D;\ M = \pm1) + C(^3P;\ M = \pm1)$ and $Fe^+(^6D;\ M = \pm2) + C(^3P;\ M = 0)$, respectively. At 5 bohr, an avoided crossing appears between

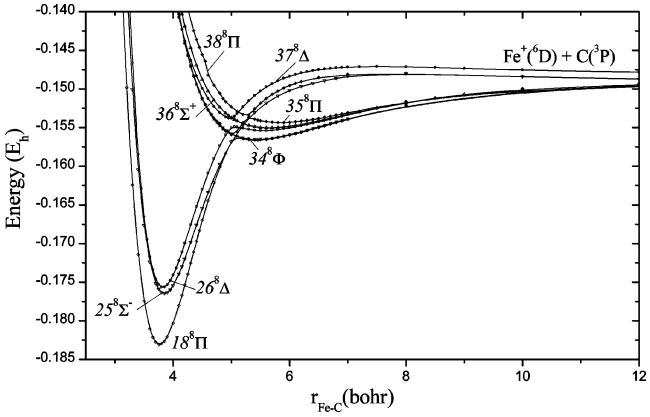

Figure 6. MRCI PECs of the octet states of the FeC^+ cation.

them, causing the mutual exchange of their characters. As a result, the $26^8\Delta(1)$ state shows two minima with the above characters and the $37^8\Delta(2)$ state has its minimum on the crossing.

V. Synopsis and Remarks

Employing multireference variational calculations, CASSCF + 1 + 2 = MRCI coupled with adequate basis sets, we have constructed potential energy curves for 40 states of the FeC^+ diatomic carbide cation. The ground state $X^2\Delta$ was also examined by the coupled-cluster CCSD(T) approach using CASSCF orbitals. It should be stressed at this point that this is the first systematic high-level ab initio work on this system, and experimental results are also very limited. Thus, it is hoped that the current study can be of considerable help in the experimental investigation of this interesting molecular cation.

A synopsis of our findings and conclusions follows.

1. The binding energies (D_0) of the $X^2\Delta$ state of FeC^+ with respect to the adiabatic fragments $Fe^+(^4F) + C(^3P)$ are 104 (105) kcal/mol. This is a D_e C-MRCI (C-MRCI+Q) value corrected for scalar relativistic effects via the DKH approximation, zero-point energy $\omega_e/2$, and BSSE. The corresponding D_0 value, but with respect to the ground-state species $Fe^+(^6D) + C(^3P)$, is 87 (92) kcal/mol. The 92 kcal/mol D_0 value compares favorably to the experimental one of 94 ± 7 kcal/mol,[6] assuming that the latter refers to ground-state fragments.

2. The first excited state, $a^4\Sigma^-$, lies 19.0 (18) kcal/mol above the $X^2\Delta$ state with $D_e = 72.2$ (76) kcal/mol at the MRCI (MRCI+Q) level and a bond distance about 0.1 Å longer than that of the X state. There is no exact analogue of the FeC^+ $a^4\Sigma^-$ state among the 41 calculated states of the neutral FeC recently reported.[2]

3. All 40 states examined are bound with respect to their ground-state fragments, with D_e's and r_e's ranging from 101 kcal/mol and 1.568 Å ($X^2\Delta$) to 3.6 kcal/mol ($38^8\Pi$ state) and 2.946 Å ($36^8\Sigma^+$ state) at the MRCI+Q level. In addition, all states correlate to the $C(^3P; M = 0, \pm1)$ atom, with the $M = 0$ carbon component forming states with the larger D_e and shorter r_e values in most of the cases.

4. For all states and for obvious reasons, the $\delta_+(d_{x^2-y^2})$ and $\delta_-(d_{xy})$ electrons remain strictly localized on the Fe atom; therefore, their participation in the bonding process is rather neutral.

5. With the exception of the octets, almost all other states are of intense multireference character, thus introducing severe technical problems and interpretational difficulties.

6. As can be seen from Figures 1 and 2, a large number of states are very close in energy, and therefore, we cannot be certain of their true sequence. The MRCI order is particularly uncertain for the pairs or group of states where the T_e's differ by about 1 mE_h. For instance, by applying the Davidson correction (+Q), the ordering of certain states is reserved. Also, the ordering is reversed by adding the zero-point energy differences, $\Delta\omega_e/2$, for the pairs $\{10^4\Sigma^-(2), 11^4\Pi(2)\}$, $\{16^4\Pi(3), 17^4\Sigma^+(1)\}$, $\{18^8\Pi(1), 19^6\Phi(1)\}$, $\{24^2\Delta(2), 25^8\Sigma^-(1)\}$, and $\{33^6\Sigma^+(2), 34^8\Phi(1)\}$ by 0.2, 0.7, 0.2, 0.3, and 0.5 kcal/mol. However, we are practically certain of the relative position of the ground state and of the first seven excited states.

Acknowledgment. The financial help of the Academy of Athens, of the Greek Ministry of Education, and of the European Union through the program PYTHAGORAS (70/3/7373) is greatly appreciated.

References and Notes

(1) (a) Kerkines, I. S. K.; Mavridis, A. *J. Phys. Chem. A* **2000**, *104*, 11777. (b) Kalemos, A.; Mavridis, A.; Harrison, J. F. *J. Phys. Chem. A* **2001**, *105*, 755. (c) Kalemos, A.; Mavridis, A. *J. Phys. Chem. A* **2002**, *106*, 3905. (d) Kerkines, I. S. K.; Mavridis, A. *Collect. Czech. Chem. Commun.* **2003**, *68*, 387. (e) Kerkines, I. S. K.; Mavridis, A. *Mol. Phys.* **2004**, *102*, 2451.

(2) Tzeli, D.; Mavridis, A. *J. Chem. Phys.* **2002**, *116*, 4901.

(3) Tzeli, D.; Mavridis, A. *J. Chem. Phys.* **2003**, *118*, 4984. Tzeli, D.; Mavridis, A. *J. Chem. Phys.* **2005**, *122*, 056101.

(4) See, for instance: Harrison, J. F. *Chem. Rev.* **2000**, *100*, 679, and references therein.

(5) Hettich, R. L.; Freiser, B. S. *J. Am. Chem. Soc.* **1986**, *108*, 2537.

(6) Angeli, C.; Berthier, G.; Rolando, C.; Sablier, M.; Alcaraz, C.; Dutuit, O. *J. Phys. Chem. A* **1997**, *101*, 7907.

(7) Hsieh, S.; Eland, J. H. D. *Int. J. Mass Spectrom. Ion Processes* **1997**, *167/168*, 415.

(8) Gutsev, G. L.; Bauschlicher, C. W., Jr. *Chem. Phys.* **2003**, *291*, 27.

(9) Moore, C. E. *Atomic Energy Levels*; NSRDS-NBS Circular No. 35; Washington, DC, 1971.

(10) Bauschlicher, C. W., Jr. *Theor. Chim. Acta* **1995**, *92*, 183.

(11) Dunning, T. H., Jr. *J. Chem. Phys.* **1989**, *90*, 1007.

(12) Werner, H.-J.; Knowles, P. J. *J. Chem. Phys.* **1988**, *89*, 5803. Knowles, P. J.; Werner, H.-J. *Chem. Phys. Lett.* **1988**, *145*, 514. Werner, H.-J.; Reinsch, E. A. *J. Chem. Phys.* **1982**, *76*, 3144. Werner, H.-J. *Adv. Chem. Phys.* **1987**, *LXIX*, 1.

(13) Docken, K.; Hinze, J. *J. Chem. Phys.* **1972**, *57*, 4928. Werner, H.-J.; Meyer, W. *J. Chem. Phys.* **1981**, *74*, 5794.

(14) Langhoff, S. R.; Davidson, E. R. *Int. J. Quantum Chem.* **1974**, *8*, 61. Blomberg, M. R. A.; Sieghbahm, P. E. M. *J. Chem. Phys.* **1983**, *78*, 5682.

(15) Werner, H.-J.; Knowles, P. J. *MOLPRO 2000*. MOLPRO 2000 is a package of ab initio programs with contributions by Amos, R. D.; Bernhardsson, A.; Berning, A.; Celani, P.; Cooper, D. L.; Deegan, M. J. O.; Dobbyn, A. J.; Eckert, F.; Hampel, C.; Hetzer, G.; Korona, T.; Lindh, R.; Lloyd, A. W.; McNikolas, S. J.; Manby, F. R.; Meyer, W.; Mura, M. E.; Nicklass, A.; Palmieri, P.; Pitzer, R.; Rauhut, G.; Schuetz, M.; Stoll, H.; Stone, A. J.; Tarroni, R.; and Thorsteinsson, T. 2000, Birmingham, UK.

(16) Brugh, D. J.; Morse, M. D. *J. Chem. Phys.* **1997**, *107*, 9772.

(17) In ref 2 (FeC), the basis set employed is [7s6p4d3f/$_{Fe}$ 4s3p2d1f/$_C$], as compared to the [7s6p4d3f2g/$_{Fe}$ 5s4p3d2f1g/$_C$] basis set presently used, except for the first three states ($X^3\Delta$, $1^1\Delta$, $2^3\Sigma^-$) where both bases have been used. Therefore, for reasons of better comparison, results from ref 2 have been "empirically" corrected when needed on the basis of differences between the two basis sets of the three states above.